2014 IEEE International Conference on Robotics & Automation (ICRA)
Hong Kong Convention and Exhibition Center
May 31 - June 7, 2014. Hong Kong, China

Backstepping Variable Structure Control of Slip-Based Kinematics and Dynamics for Improved AGV Cornering Performance

Ming Xin, and Mark A. Minor, *Member, IEEE*

***Abstract*—Tracking accuracy in ground vehicle path following is an important topic addressed by vehicle steering control. While several controllers exist, this controller aims to provide improved path following while cornering on sloped terrain. Towards this goal, this work develops a new kinematic controller that considers the effect of slip and a new dynamic controller that better compensates modelling error and actuator disturbances. The kinematic controller uses a new kinematic model and applies backstepping architecture with variable structure control manifolds to assure smooth and graceful yaw rate commands. The dynamic controller is also based upon backstepping, but introduces integrator states to the architecture and derives a new controller to improve yaw rate tracking. Simulations and field experiments demonstrate resulting performance improvements, which are compared to prior work to highlight contributions of this work.**

I. Introduction

GRACEFUL and robust steering control of full size ground vehicles is critical for passenger comfort and safety, which impacts both Automated Ground Vehicle (AGV) and driver assistance technology. Numerous steering controllers have been developed, but many of them are focused on sensor-based navigation, such as DARPA Urban Challenge vehicles [1] or Google Car [2], or kinematic control [3]. Although sensor-based navigation can consider driving safety from a planning perspective, it does not consider vehicle response while applying the steering commands. On the other hand, kinematic-based steering control can work at low speeds, but it is inappropriate for high speeds and varying conditions. Vehicle side slip determines dynamic interactions between the vehicle and ground, which must be considered in order to allow vehicles to respond appropriately to their environment. Control of slip is critical for vehicle maneuverability, accurate path following, and graceful motion. Thus, a combined kinematic and dynamic controller is necessary to consider steering commands, vehicle yaw rate, and side slip.

This paper presents a novel steering controller to improve path following accuracy. Fig 1 presents the architecture of this steering controller and the symbol definitions refer to Sec II and III. Since slip is typically a major source of tracking error, this work considers slip-based kinematics in order to derive yaw rate commands for path following. A slip-yaw dynamic model then provides a basis for deriving steering rate commands and a sensor based observer provides estimates of slip and yaw rate for output feedback control. The kinematic controller is based upon a backstepping approach where lateral tracking error is first regulated by heading. Backstepping then considers simultaneous regulation of heading and lateral tracking error using yaw rate commands. Side-slip is treated as a tracking error term at this level where a Variable Structure Control (VSC) approach is used to derive graceful and robust yaw rate commands that drive tracking error to zero despite slip and external disturbances.

The dynamic controller then uses a backstepping approach where yaw-rate tracking is considered first in order to derive steering angles while considering side-slip. Integral control is added to compensate modelling errors, external disturbances, and actuator backlash for improved tracking. Steering angle references are then backstepped into a steering rate controller so that the steering actuator provides concurrent tracking of both yaw rate and steering angle while considering the effect of side-slip and the actuator dynamics. Integral control is added to compensate actuator tracking error caused by actuator servo loops and loads acting on the actuator. An observer from [4-6] provides estimates of side slip and yaw rates in order to achieve sensor based output feedback control.

While many researchers have examined AGV control from a kinematics perspective, a limited number have considered dynamics with kinematics, and some just consider dynamics. For example, Stanford has relied heavily upon kinematic control, but has provided some consideration of dynamics. In [7], they consider tire slip angle and cornering stiffness to determine discrete sets of feasible steering angles which planning algorithms then select from. They achieved good accuracy in off-road trajectory-tracking, but did not consider graceful motion nor active control of vehicle dynamics. Werling [3] provides a tighter integration by using a longitudinal dynamic model in addition to a standard bicycle kinematic model, but slip is not considered. This improves tracking capability where speed variations are small, but it may cause a vehicle to become unstable at higher speeds under varying conditions. Others consider dynamic control, but only provide simulation results [8, 9].

Only a few researchers [10, 11] have considered kinematic and dynamics models similar to our own in [4-6], and results from these works are limited. Wang et al [10] uses a similar control structure, but basic PD control for kinematics and SMC for dynamics, where steering angle is used as the control input. PD control results in sensitivity to initial conditions and limited ability to reject disturbances and compensate for slip.

* This research is supported by University of Utah
Ming Xin is with the University of Utah, Salt Lake City, Utah USA (E-mail: ming.xin@ utah.edu).
Mark Minor is with University of Utah, Salt Lake City, Utah 84112 USA. (E-mail: mark.minor@utah.edu).

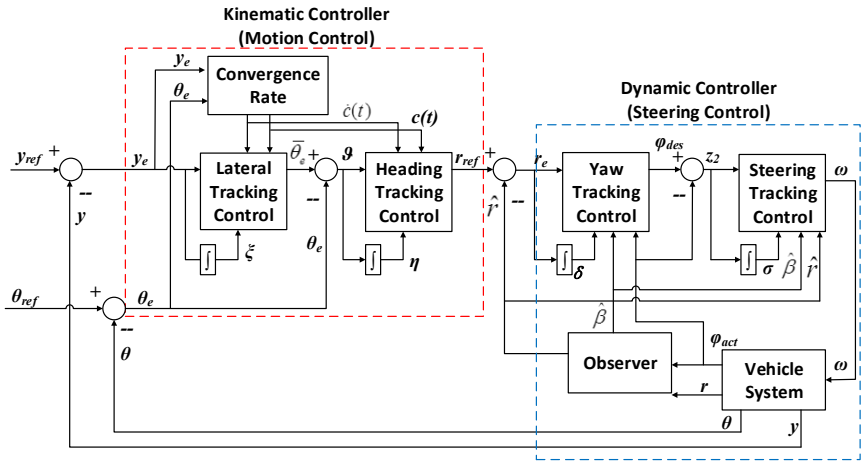

Fig 1. Control system block diagram.

Likewise, vehicle handling capability and actuator limitations are not considered, and the tire-ground model used in their dynamic controller would be difficult to implement in a full-size vehicle. Lastly, only simulation results are provided and hence practicality of this approach is not demonstrated. Raffo et al [11] uses an architecture and slip-yaw model similar to our own, but uses more sophisticated predictive control compared to [10]. Experimental results are also provided, but the platform is a smaller Mini-baja vehicle, and side slip and steering dynamics are ignored due to computational limitations. As a result, the vehicle operates at low speeds (1 to 2.77 m/s) to maintain stability and tracking accuracy, and slip is ultimately ignored in their results.

This paper shares some features and approaches with our prior work [4-6], such as the multi-tiered control architecture, the VSC approach in the kinematic controller, and the backstepping approach in the dynamic controller. However, [4-6] do not consider the effect of side slip in the vehicle kinematics, whereas this paper does. As a result, this paper presents new kinematic models considering slip and their new controllers. Our prior work used either Sliding Mode Control (SMC) [4, 5] or VSC [6] to design the kinematic controller, but this did not consider possible model error in this manifold coupling. This paper uses a backstepping approach to better assure sequential convergence of lateral error and heading error despite possible modelling error. This paper applies similar VSC manifolds from [6] to achieve smooth and graceful motion, but the resulting controller is new. Our prior work [5, 6] also used a backstepping approach in the dynamic controller to realize reference yaw rates, but this work adds integral terms to improve tracking and results in a new backstepping controller. This paper and our prior work both use the same high gain observer to estimate slip and yaw rate.

The structure of the paper is as follows. Section II provides the revised kinematic model and the dynamic model that form the basis of the controllers. The new kinematic controller is presented in Section III and the new dynamic controller is presented in Section IV. Simulation and experimental results highlighting resulting performance improvements are shown in Sections V and VI, respectively. Concluding remarks are provided in Section VII.

II. Modeling

A. Kinematic Model

As in [4-6], the vehicle kinematics are demonstrated as Fig 2. Likewise, the vehicle kinematic model is described by a classic non-slip bicycle model as:

$$\dot{x} = V\cos\theta \tag{1}$$

$$\dot{y} = V\sin\theta \tag{2}$$

$$\dot{\theta} = (V/L)\cdot\tan\varphi = r \tag{3}$$

$$\dot{\varphi} = \omega \tag{4}$$

where $P_a = [x, y, \theta]$ is the posture of the vehicle. The vehicle heading angle is θ, and its time derivative is yaw rate, r. The front steering angle is φ, while its time derivative is steering rate, ω. The longitudinal and lateral positions in the global frame XOY are x and y. The vehicle forward speed is V.

The lateral tracking error, y_e is defined as the closest distance from P_a to the reference path. The reference yaw rate is $\dot{\theta}_{ref} = \kappa V = V/R$, where κ is the reference path curvature and a reciprocal of radius of path, R.

Because the longitudinal motion is insignificant to path following motion, we thus neglect (1) and only consider (2) ~(4) in this paper. (4) describes the steering actuator dynamics and steering capability and is split from kinematics and added to dynamics as augmented dynamic states. The kinematic model expressed in tracking error form is:

$$\dot{\theta}_e = r - \kappa V \tag{5}$$

$$\dot{y}_e = V\sin\theta_e \tag{6}$$

where θ_e is the heading error, and $\theta_e = \theta - \theta_{ref}$.

(5) and (6) do not consider the impact of side slip to kinematics, which is a critical reason to cause lateral tracking error in our prior work. Thus, we modify the kinematic model to become a slip-based kinematic model by including the side slip disturbance term as:

$$\dot{y}_e = V\sin\bar{\theta}_e \tag{7}$$

$$\theta_e = \bar{\theta}_e + \vartheta \tag{8}$$

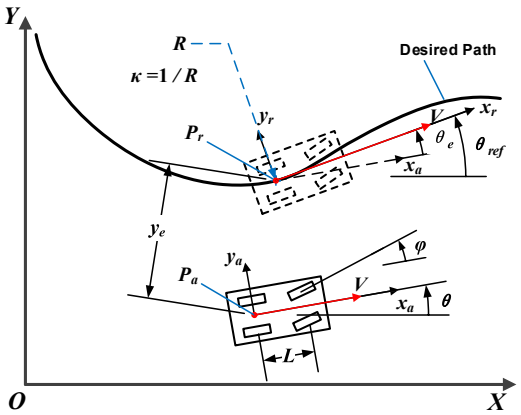

Fig 2: Vehicle Kinematic Model.

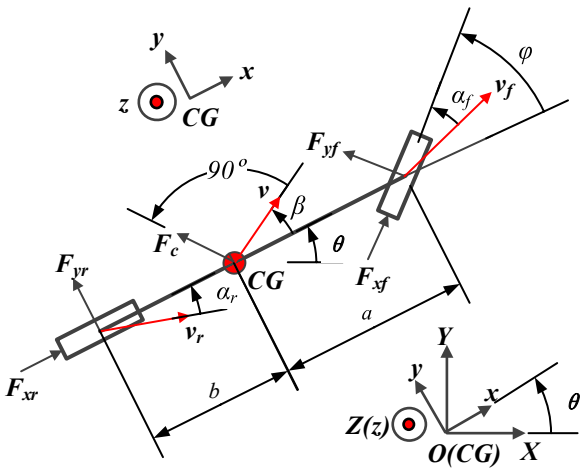

Fig 3: Vehicle Dynamic Model.

$$\dot{\theta}_e = r - \kappa V \tag{9}$$

where $\bar{\theta}_e$ is a nominal heading error; ϑ is a side slip disturbance term. The actual heading error is θ_e. The new slip-based kinematic model is applied for the kinematic controller design.

B. Dynamic Model

Likewise, the vehicle dynamic model is approximated by a slip and yaw based bicycle model as in Fig 3, where we introduce a cornering stiffness model to describe side slip, β, yaw rate, r, and lateral dynamics.

Unlike prior work, we now can consider the kinematic velocity, $V = v$, which reduces the uncertainty that existed between kinematic and dynamic models in [4-6]. The variation of vehicle velocity is small and slow and treated as uncertainty, which is an appropriate assumption to common high-speed or low-speed driving. By including the steering actuator dynamics (4), the vehicle dynamic model is described as:

$$\dot{\beta} = -\frac{(C_f + C_r)}{mv}\beta - \left(1 + \frac{C_f \cdot a - C_r \cdot b}{mv^2}\right) r + \frac{C_f}{mv}\varphi \tag{10}$$

$$\dot{r} = -\frac{C_f \cdot a - C_r \cdot b}{J}\beta - \frac{C_f \cdot a^2 + C_r \cdot b^2}{Jv} r + \frac{C_f \cdot a}{J}\varphi \tag{11}$$

$$\dot{\varphi} = \omega \tag{12}$$

where C_f and C_r are the actual cornering stiffness of front and rear tires and defined as: $C_f = \mu C_{f0}$ and $C_r = \mu C_{r0}$ where μ is road coefficient. C_{f0} and C_{r0} are cornering stiffness on an ideal road (i.e. $\mu = 1$). m and J are mass and inertia. a and b are distances from CG location to front and rear axle center. Note that the vehicle velocity is assumed positive, $v > 0$. In order to start from rest where $v = 0$, the vehicle needs to be driven for a while before the controller and observer are engaged. (10) ~ (12) are represented in a simplified form:

$$\dot{\beta} = a_{11}\beta + a_{12} r + b_{11}\varphi \tag{13}$$

$$\dot{r} = a_{21}\beta + a_{22} r + b_{21}\varphi \tag{14}$$

$$\dot{\varphi} = \omega \tag{15}$$

III. Kinematic Controller

The goal of the kinematic controller is to provide yaw rate commands that drive lateral and heading tracking error to zero gracefully. However, due to the simplification of side slip in describing vehicle kinematics, accurate tracking performance cannot be sufficiently achieved. We thus remodel the vehicle kinematics by addressing a slip-based kinematic model to compensate the impact of side slip to lateral tracking error.

The yaw rate, r, still serves as the kinematic control command for its intuitive relation to side slip, vehicle steering, and graceful motion. The current kinematic model is restructured in a cascading form by including integrators:

$$\dot{\xi} = y_e \tag{16}$$

$$\dot{y}_e = V \sin\bar{\theta}_e \tag{17}$$

$$\dot{\eta} = \vartheta \tag{18}$$

$$\dot{\theta}_e = r - \kappa V \tag{19}$$

We first consider (16) and (17) and treat the nominal heading error, $\bar{\theta}_e$, as a virtual control input. The Lyapunov candidate function V_1 is selected: $V_1 = \frac{K_{i1}\xi^2}{2} + \frac{y_e^2}{2}$, where $V_1 : D_1 \to \Re^2$ is a continuously differentiable positive definite function on a domain, D_1, containing the origin, $x_1 \equiv 0$, where $x_1 = [\xi \quad y_e]^T$. The domain D_1 is defined as: $D_1 = \{x_1 \in \Re^2 | -a_1 < (K_{i1}\xi^2 + {y_e}^2) < a_1, a_1 \in \Re^2\}$

The time derivative of V_1 is: $\dot{V}_1 = K_{i1}\xi y_e + y_e(V \sin\bar{\theta}_e)$, by designing the virtual control input $\bar{\theta}_e$ as:

$$\bar{\theta}_e = -\arcsin\left(\frac{K_{i1}\xi + c_1(t) y_e}{V}\right) \tag{20}$$

to achieve $\dot{V}_1 = -c_1(t){y_e}^2$. Since $c_1(t)$ is a set of positive numbers, K_{i1} is an positive integral gain, $\dot{V}_1 = -c_1(t){y_e}^2 \le 0$ in the domain, D_1. If a domain S_1 is set as $\{x_1 \in D_1 | \dot{V}_1(x_1) = 0\}$, no solution can stay identically in S_1, other than the trivial solution $x_1 \equiv 0$. Based on Barbashin's theorem following LaSalle's invariance principle [12], the origin x_1 is asymptotically stable. Note that a saturation function is applied within the arcsin term of (20) to assure it is bounded within [-1, 1].

As in Section II, the vehicle velocity in (20) is also assumed $V > 0$, while the vehicle needs to be driven to achieve the threshold velocity to avoid singularity before the kinematic controller is fully engaged. In the field experiments, the threshold velocity is $V = 0.5$ m/s

The time derivative of θ is:

$$\dot{\vartheta} = \dot{\theta}_e - \dot{\bar{\theta}}_e = r - \kappa V + \arcsin\left(\frac{K_{i1}\xi + c_1(t) y_e}{V}\right)' \tag{21}$$

Rearranging(16), (17), (18), and (21) in a cascading form:

$$\dot{\xi} = y_e \tag{22}$$

$$\dot{y}_e = -c_1 y_e - K_i \xi + \vartheta \tag{23}$$

$$\dot{\eta} = \vartheta \tag{24}$$

$$\dot{\vartheta} = r - \kappa V + \frac{\dot{c}_1(t) y_e + c(t)\dot{y}_e + K_{i1} y_e}{V\sqrt{1-\left(\frac{c_1(t) y_e + K_{i1}\xi}{V}\right)^2}} \quad (25)$$

Selecting the composite Lyapunov candidate function V_{c1} as:

$$V_{c1} = \frac{K_{i1}}{2}\xi^2 + \frac{1}{2} y_e^{\,2} + \frac{K_{i2}}{2}\eta^2 + \frac{1}{2}\vartheta^2 \quad (26)$$

where $V_{c1}: D_2 \rightarrow \Re^4$ is a continuously differentiable positive definite function on a domain, D_2, containing the origin, $x_2 \equiv 0$, where $x_2 = \begin{bmatrix}\xi & y_e & \eta & \vartheta\end{bmatrix}^T$. The domain D_2 is defined as: $D_2 = \{x_2 \in \Re^4 \mid -a_2 < (K_{i1}\xi^2 + y_e^2 + K_{i2}\eta^2 + \vartheta^2) < -a_2,\ a_2 \in \Re^4\}$. The time derivative of V_{c1} is: $\dot{V}_{c1} = K_{i1}\xi y_e + y_e\dot{y}_e + K_{i2}\eta\dot{\eta} + \vartheta\dot{\vartheta}$, substituting (22) ~ (25) in $\dot{V}_{c1}$ and simplifying:

$$\dot{V}_{c1} - c_1 y_e^{\,2} + \vartheta(y_e + K_{i2}\eta + \dot{\theta}) \quad (27)$$

Let $y_e + K_{i2}\eta + \dot{\theta} = -K_{p2}\vartheta$, such that (27) becomes $\dot{V}_{c1} = -c_1(t)y_e^2 - K_{p2}\vartheta^2 \leq 0$ in the domain D_2. If a domain S_2 is set as $\{x_2 \in D_2 \mid \dot{V}_{c1}(x_2) = 0\}$, no solution can stay identically in S_2, other than the trivial solution $x_2 \equiv 0$. Based on Barbashin's theorem following LaSalle's invariance principle [12], the origin x_2 is asymptotically stable. Thus, the yaw rate, r, should be

$$r = \kappa V - \frac{\dot{c}_1(t) y_e + c(t)\dot{y}_e + K_{i1} y_e}{V\sqrt{1-\left(\frac{c_1(t) y_e + K_{i1}\xi}{V}\right)^2}} - K_{p2}\vartheta - K_{i2}\eta - y_e \quad (28)$$

In principle, (28) is able to satisfy the request to provide appropriate yaw rate commands by considering the impact of side slip. However, based upon preliminary simulations, it has limited tuning capability to path manifolds for achieving graceful motion. Also, (28) is insufficient to provide robustness to uncertainties caused by the interaction of vehicle kinematics and dynamics. Thus, we revisit (25) and (28) and redesign the control law by embedding a variable structure control (VSC) approach for solving these two issues.

Selecting the path manifold as:

$$S_{kin} = \theta_e + \arcsin\left(\frac{c_1(t) y_e + K_i\xi}{V}\right) \quad (29)$$

The time derivative of S_{kin} is:

$$\dot{S}_{kin} = r - \kappa V + \arcsin\left(\frac{K_{i1}\xi + c_1(t) y_e}{V}\right)' \quad (30)$$

which is the same as (25). So, the Lyapunov candidate function is selected: $V_2 = (S_{kin})^2/2$, while the time derivative of V_2 is:

$$\dot{V}_2 = S_{kin}\cdot\dot{S}_{kin} = S_{kin}(r - \kappa V + \arcsin\left(\frac{K_{i1}\xi + c_1(t) y_e}{V}\right)') \quad (31)$$

where, V_2 is positive definite, for $S_{kin} \in \Re^2, \forall\, S_{kin} \neq 0$.

Referring to [6], we consider the yaw rate, r, in (31) as the temporary control input, r_{temp} and designed it as:

$$r_{temp} = -\left(\rho_{kin} + \psi_{kin}\right)\tanh\left(\frac{S_{kin}}{\varepsilon_{kin}}\right) \quad (32)$$

such that $\dot{V}_2$ is negative definite, for $S_{kin} \in \Re^2, \forall\, S_{kin} \neq 0$, where $\rho_{kin} = \frac{|\dot{c}(t) y_e + c(t)\dot{y}_e + K_{i1} y_e|}{\left|V\sqrt{1-((c_1(t) y_e + K_{i1}\xi)/V)^2}\right|}$, which is the lower bound of the robust term. ψ_{kin} is an arbitrary positive number to assure Lyapunov stability. The hyperbolic function is used to remove "chattering", where ε_{kin} determines the magnitude of the convergence boundary layer. By applying (32) in (28), the kinematic control law becomes,

$$r = \kappa V - (\rho_{kin} + \psi_{kin})\tanh\left(\frac{S_{kin}}{\varepsilon_{kin}}\right) - K_{p2}\vartheta - K_{i2}\eta - y_e \quad (33)$$

Compared to (28), (33) is more conservative but provides path manifold tuning ability and robustness by embedding a VSC approach in the backstepping control frame.

IV. Dynamic Controller

The dynamic controller generates steering commands to create the yaw rate specified by the kinematic controller. This yaw rate is defined as, r_{ref}, according to (33). The actual yaw rate from the dynamics is now referred to, r. The yaw rate tracking error is r_e, where $r_e = r - r_{ref}$.

The yaw rate tracking error models are derived as (34) and (35), while the desired steering angle, φ_{des}, is the control input. The integral of yaw error, δ, is used to compensate steady state yaw rate tracking error caused by modeling error and external uncertainty. Despite of these uncertainty in the vehicle dynamics, the yaw rate command terms, r_{ref} and its time derivatives are highly nonlinear. Thus, although the vehicle dynamic model is linearized, the robust backstepping strategy is applied to the dynamic controller for improving control performance in practice.

$$\dot{r}_e = a_{21}\beta + a_{22} r_e + (a_{22} r_{ref} - \dot{r}_{ref}) + b_{21}\varphi_{des} \quad (34)$$

$$\dot{\delta} = r_e \quad (35)$$

The Lyapunov candidate function is selected as $V_3 = \frac{r_e^2}{2} + \frac{K_{i3}\delta^2}{2}$. Likewise, $V_3: D_3 \rightarrow \Re^2$ is a continuously differentiable positive definite function on a domain, D_3, containing the origin, $x_3 \equiv 0$, where $x_3 = [r_e \quad \delta]^T$. The domain D_3 is efined as $D_1 = \{x_3 \in \Re^2 \mid -a_3 < (r_e^{\,2} + K_{i3}\delta^2) < a_3, a_3 \in \Re^2\}$, where a_3 can be an arbitrarily large constant.

According to (33), $\dot{r}_{ref}$ contains undifferentiable terms, while these terms are neglected when the controller is in simulation and experiments. The impact of these terms is treated as uncertainty and perturbation to the dynamic system, which can be stabilized by the robust controller.

The time derivative of V_3 is:

$$\dot{V}_3 = r_e\cdot\dot{r}_e + K_{i3}\delta\cdot r_e = r_e(\dot{r}_e + K_{i3}\delta) \quad (36)$$

Let $\dot{r}_e + K_{i3}\delta = -(K_{p3} - a_{22})r_e$ such that $\dot{V}_3 = -(K_{p3} - a_{22})r_e^2 \leq 0$ in the domain, D_3, where K_{p3} is a positive proportional gain and $K_{p3} > a_{22}$. If a domain S_3 is set as $\{x_3 \in D_3 \mid \dot{V}_3(x_3) = 0\}$, no solution can stay identically in S_3, other than the trivial solution $x_3 \equiv 0$. Based on Barbashin's theorem following LaSalle's invariance principle [12], the origin x_3 is asymptotically stable. Thus, the control input, φ_{des}, should be:

$$\varphi_{des} = -\frac{a_{21}\beta + a_{22}r_{ref} - \dot{r}_{ref} + K_{p3}r_e + K_{i3}\delta}{b_{21}} \quad (37)$$

In addition, (15) provides the steering angle that fundamentally decides the yaw rate in the kinematic model. Both steering angle and yaw rate are achieved by the vehicle dynamics to extend the dynamics by considering actuator capability, where (15) is represented: $\dot{\varphi}_{act} = \omega$. The steering tracking error is defined as z_2, where $z_2 = \varphi_{act} - \varphi_{des}$. Another integral state, σ, is introduced to further reduce the steady-state steering tracking error. The extended dynamic model is then defined as,

$$\dot{\delta} = r_e \quad (38)$$

$$\dot{r}_e = -(K_{p3} - a_{22})r_e + z_2 \quad (39)$$

$$\dot{\sigma} = z_2 \quad (40)$$

$$\dot{z}_2 = \dot{\varphi}_{act} - \dot{\varphi}_{des} = \omega + \frac{a_{21}\dot{\beta} + a_{22}\dot{r}_{ref} - \ddot{r}_{ref} + K_{p3}\dot{r}_e + K_{i3}r_e}{b_{21}} \quad (41)$$

Backstepping approach is again applied, where the steering rate, ω, is now control input. The composite Lyapunov candidate function V_{c2} is:

$$V_{c2} = \frac{1}{2}r_e^2 + \frac{K_{i3}}{2}\delta^2 + \frac{1}{2}z_2^2 + \frac{K_{i4}}{2}\sigma^2 \quad (42)$$

where, $V_{c2} : D_4 \to \Re^4$ is a continuously differentiable positive definite function on a domain, D_4, containing the origin, $x_4 \equiv 0$, where $x_4 = \begin{bmatrix}\delta & r_e & z_2 & \sigma\end{bmatrix}^T$. The domain D_4 is defined as: $D_4 = \{x_4 \in \Re^4 | -a_4 < (r_e^2 + K_{i3}\delta^2 + z_2^2 + K_{i4}\sigma^2) < a_4,\ a_4 \in \Re^4\}$.

The time derivative is:

$$\dot{V}_{c2} = r_e \cdot \dot{r}_e + K_{i3}\delta\dot{\delta} + z_2 \cdot \dot{z}_2 + K_{i4}\sigma \cdot \dot{\sigma} \quad (43)$$

Substituting (38) ~(40) to (43) and simplifying,

$$\dot{V}_{c2} = -(K_{p3} - a_{22})r_e^2 + z_2(\dot{z}_2 + K_{i4}\sigma + r_e) \quad (44)$$

Let $\dot{z}_2 + K_{i4}\sigma + r_e = -K_{p4}z_2$, so $V_{c2} = -(K_{p3} - a_{22})r_e^2 - K_{p4}z_2^2 \le 0$ in the domain D_4. If a domain S_4 is set as $\{x_4 \in D_4 | \dot{V}_4(x_4) = 0\}$, no solution can stay identically in S_4, other than the trivial solution $x_4 \equiv 0$. Based on Barbashin's theorem following LaSalle's invariance principle [12], the origin x_4 is asymptotically stable. Thus, the steering rate, ω, is,

$$\omega = -\frac{a_{21}\dot{\beta} + a_{22}\dot{r}_{ref} - \ddot{r}_{ref} + K_{p3}\dot{r}_e + (K_{i3} + b_{21})r_e}{b_{21}} - K_{p4}z_2 - K_{i4}\sigma \quad (45)$$

where (45) is the dynamic control law.

A high gain observer similar to [4-6] is used to derive states estimates,

$$\begin{aligned}\dot{\hat{\beta}} &= a_{11}\hat{\beta} + a_{12}\hat{r} + b_{11}\varphi_{act} + h_1(r - \hat{r}) \\ \dot{\hat{r}} &= a_{21}\hat{\beta} + a_{22}\hat{r} + b_{21}\varphi_{act} + h_2(r - \hat{r})\end{aligned} \quad (46)$$

where $\hat{\beta}, \hat{r}$ are side slip and yaw rate estimates; h_1 , h_2 are observer gains, which are defined,

$$h_1 = \frac{1}{\varepsilon^2}, h_2 = \frac{2}{\varepsilon} \quad (47)$$

ε is an arbitrary positive number and is tuned to reduce estimation error. However, decreasing ε below 0.1 does not improve estimates and excites vehicle dynamics in field experiments, which is likely due to limited sampling rate. (46) is used by the dynamic controller for output feedback control.

Based upon the prior work [4-6], the output feedback control law can be represented as:

$$\omega = -\frac{a_{21}\dot{\hat{\beta}} + a_{22}\dot{\hat{r}}_{ref} - \ddot{\hat{r}}_{ref} + K_{p3}\dot{\hat{r}}_e + (K_{i3} + b_{21})\hat{r}_e}{b_{21}} - K_{p4}\hat{z}_2 - K_{i4}\hat{\sigma} \quad (48)$$

V. Simulation

The vehicle parameters maintain their definition in Section II. The nominal values are the same as [6]: C_f = 110000 *N/rad*, C_r = 110000 *N/rad*; a = 1.2 *m*, b = 1.8 *m*; m = 2300 *kg*, J = 4500 *kg.m*^{2}. These values are also used in observer and controller in simulations and field experiments.

The simulated vehicle system is perturbed to evaluate robustness such that C_f = 230000 *N/rad*, C_r = 200000 *N/rad*; a = 1.3 *m*, b = 1.7 *m*; m = 2540 *kg*, J = 5000 *kg.m*^{2}. Wind effects are simulated by drag coefficient 0.41 *N/(m/s)*^{2} and wind lift coefficient 0.005 *N/(m/s)*^{2}. Differences between

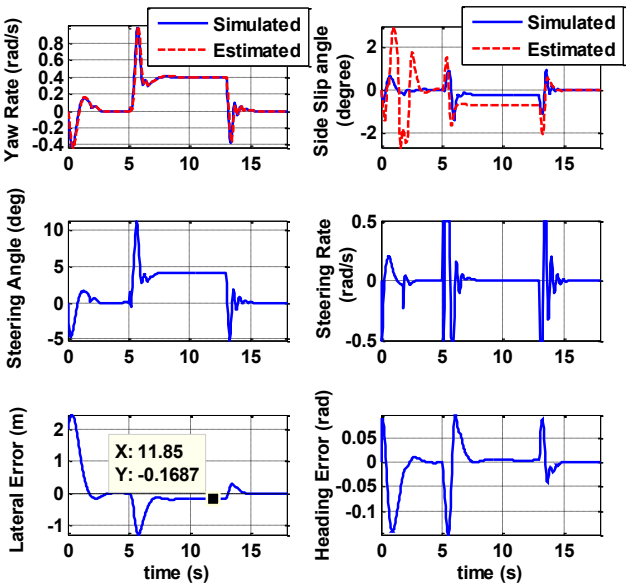

Fig 4: V = 20 *m/s* (Performed by Steering Controller in [6]).

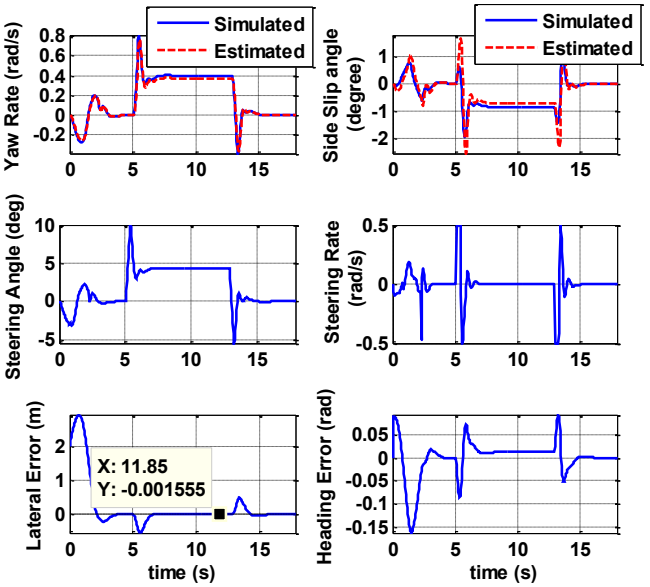

Fig 5: V = 20 *m/s* (Performed by current Steering Controller).

nominal and simulated systems or actual vehicle systems create uncertainty and disturbances in the controller and observer. To compare the current steering controller with [6], all parameters are set identical to [6]: the vehicle forward speed $V = 20$ m/s, the road coefficient $\mu = 0.8$. The initial error for simulation is $[\theta_e \quad y_e] = [0.0873 \quad 2]$. The designated path is still "U" shaped with two 100-meter straight paths and one radius of 50-m and a 180-degree arc path.

Fig 4 and Fig 5 demonstrate the control performance of our current steering controller and the prior steering controller in [6]. Obviously, the current steering controller based on slip-based kinematics provides better path-following performance in cornering. Moreover, due to the effect of integrator states, the performance of side slip estimates are also improved. The control commands have less oscillation on the places of path curvature discontinuity compared with the steering control from [6]. These features present that the slip-based steering controller is capable of achieving accurate and graceful motion in following a given path.

VI. Experiments

The testing platform and field environment are the same as in [4-6], where GPS is used for sensing vehicle posture. A digital gyroscope is used to sense vehicle yaw rate and reduce noise in the yaw rate and side slip estimates. Unlike [5, 6], the steering rate signals are made available.

Field tests are similar to [6] and simulations. However, some necessary differences exist. The 10% slope of terrain is still added to this automated vehicle and leads to non-trivial gravity disturbance in the downhill and uphill driving. Due to the limited field (parking lot), this paper only presents 1.5 ~ 3 m/s low-speed experimental results for validation.

Comparing the measured yaw rate signals to the estimated ones, Fig 6, note that differences are very small. This hints that the estimation of side slip is accurate and close to the true value. Similarly, the actual steering rate is close to the desired steering rate command from the dynamic controller. This demonstrates the effectiveness of the backstepping and steering actuator controllers. Likewise, the steering commands are more easily achieved, which reduces overshoot. This proves the necessity of considering steering actuator dynamics in the steering controller design. Finally, heading and lateral error are driven to zero, with some sensor noise shown, which is a notable improvement over [6].

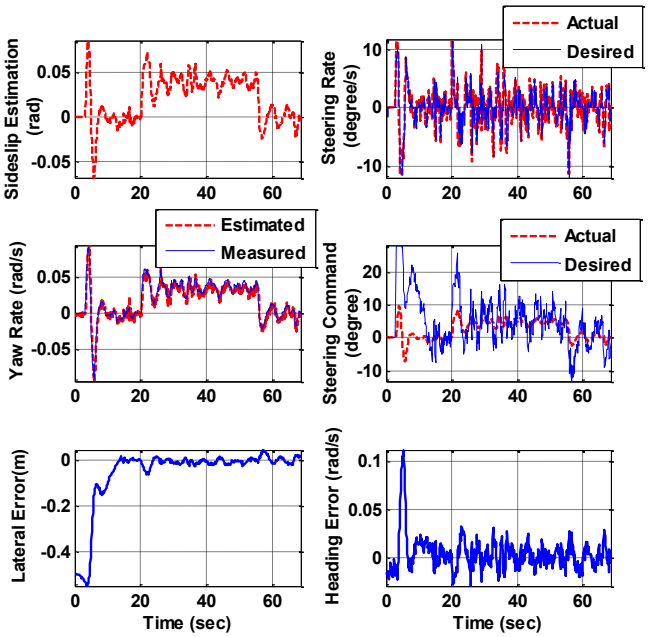

Fig 6: Experimental Results (V =1.5~3 *m/s*)

VII. Conclusion

This paper presents a slip-based backstepping variable structure steering controller for Autonomous Ground Vehicles. This algorithm considers the significant impact of side slip in improving vehicle tracking performance. The simulations demonstrate that the tracking error has been significantly reduced compared to our prior work. Field experiments validate simulations by demonstrating very small tracking error compared to prior work. Future work will provide a stability analysis including kinematics and dynamics. Experiments will be operated by applying different paths at different forward speeds.

References

[1] M. Montemerlo, J. Becker, S. Bhat, H. Dahlkamp, D. Dolgov, S. Ettinger, et al., "Junior: the Stanford entry in the urban challenge," Journal of Field Robotics, vol. 25, pp. 569-97, 2008.

[2] J. J. Zhu, M. Montemerlo, C. Urmson, and A. Chatham, "Object Detection and Classification for Autonomous Vehicles," U.S.A. Patent, 2012.

[3] M. Werling, L. Groll, and G. Bretthauer, "Invariant Trajectory Tracking With A Full-size Autonomous Road Vehicle," IEEE Trans. on Rob., vol. 26, pp. 758-65, 2010.

[4] M. Xin and M. Minor, "A multi-tiered robust steering controller based on yaw rate and side slip estimation," in 2011 IEEE/RSJ Int. Conf. on Intelligent Robots. and Systems, San Francisco, CA, USA, 2011, pp. 292-7.

[5] M. Xin and M. Minor, "Backstepping Vehicle Steering Controller Using Integral and Robust Control Based on Dynamic State Estimation," in 2012 IEEE/RSJ Int. Conf. on Intelligent Robots and Systems, Vilamoura, Algarve, Portugal, 2012.

[6] M. Xin and M. Minor, "Variable Structure Backstepping Control via Hierarchal Manifolds Set for Graceful Ground Vehicle Path Following," in 2013 IEEE Int. Conf. on Robotics and Automation, Karlsruhe, Germany, 2013.

[7] G. M. Hoffmann, C. J. Tomlin, M. Montemerlo, and S. Thrun, "Autonomous automobile trajectory tracking for off-road driving: Controller design, experimental validation and racing," in 2007 American Control Conf., New York, NY, USA, 2007, pp. 2296-2301.

[8] J. Villagra, B. d'Andrea-Novel, H. Mounier, and M. Pengov, "Flatness-based vehicle steering control strategy with SDRE feedback gains tuned via a sensitivity approach," IEEE Transactions on Control Systems Technology, vol. 15, pp. 554-65, 05/ 2007.

[9] L. Menhour, B. D'Andrea-Novel, M. Fliess, and H. Mounier, "Coupled nonlinear vehicle control: Flatness-based setting with algebraic estimation techniques," Control Engineering Practice, vol. 22, pp. 135-146, 2014.

[10] J. Wang, J. Steiber, and B. Surampudi, "Autonomous ground vehicle control system for high-speed and safe operation," in 2008 American Control Conf., Seattle, WA, USA, 2008, pp. 218-223.

[11] G. V. Raffo, G. K. Gomes, J. E. Normey-Rico, C. R. Kelber, and L. B. Becker, "A predictive controller for autonomous vehicle path tracking," IEEE Trans. on Intelligent Transportation Systems, vol. 10, pp. 92-102, 2009.

[12] H. K. Khalil, Nonlinear Systems, 3rd ed. Upper Saddle River, New Jersey: Pearson Education Int'l, 2000.